JOURNAL OF GUIDANCE, CONTROL, AND DYNAMICS
Vol. 30, No. 2, March–April 2007

Refined Solar Sail Force Model with Mission Application

Giovanni Mengali* and Alessandro A. Quarta†
University of Pisa, 56122 Pisa, Italy
Christian Circi‡
Scuola di Ingegneria Aerospaziale, 00184 Rome, Italy
and
Bernd Dachwald§
DLR, German Aerospace Center, 51147 Cologne, Germany

DOI: 10.2514/1.24779

The aim of this paper is to propose a refined mathematical model for describing the acceleration experienced by a solar sail. Unlike the conventional model characterized by constant coefficients, the force coefficients of the sail are now assumed to depend on the light incidence angle, the sail surface roughness, and the sun–sail distance. The new model is elaborated with the support of experimental data that show how the main variable affecting the force coefficients is the light incidence angle. To emphasize the differences between the refined force model with respect to the conventional one, a comparison is established through the analysis of a circle-to-circle interplanetary rendezvous problem between coplanar orbits. The problem is solved using an indirect approach and the optimal steering law is approximated in polynomial form. A number of optimal trajectories toward Mars and Venus are simulated and the results obtained are discussed as a function of the dimensionless sail loading parameter and the sail surface roughness.

Nomenclature

A	=	sail area
$\boldsymbol{a}$	=	sailcraft propulsive acceleration
a_c	=	characteristic acceleration
B	=	non-Lambertian coefficients
b_1, b_2, b_3	=	force coefficients
c	=	speed of light in vacuum
c_0, c_1, c_2	=	polynomial coefficients; see Eq. (8)
d_i	=	polynomial coefficients ($i = 0, 4, 5, 6$); see Eq. (10)
e_i	=	polynomial coefficients ($i = 1, \ldots, 4$); see Eq. (35)
f_ϵ	=	coefficient; see Eq. (6)
$\mathcal{H}$	=	Hamiltonian
$\mathcal{H}'$	=	portion of $\mathcal{H}$ that explicitly depends on the controls
h	=	root mean square value of the surface roughness
J	=	performance index
m	=	sailcraft mass
$\hat{\boldsymbol{n}}$	=	sail normal unit vector
P	=	solar radiation pressure
$\boldsymbol{r}$	=	position vector ($r \triangleq \lvert\boldsymbol{r}\rvert$)
s	=	specular reflection factor
T	=	sail equilibrium temperature
$\tilde{T}$	=	reference temperature
$\mathcal{T}_\odot$	=	polar inertial frame
t	=	time
u	=	radial velocity
v	=	circumferential velocity
α	=	cone angle
α_λ	=	primer vector cone angle
β	=	lightness number
β_σ	=	dimensionless sail loading
ϵ	=	emissivity
θ	=	polar angle
λ	=	adjoint variable
$\boldsymbol{\lambda}_v$	=	primer vector
μ	=	gravitational parameter
ρ	=	reflection coefficient
σ	=	sail loading
σ^*	=	reference sail loading
$\tilde{\sigma}$	=	Stefan-Boltzmann constant

Superscript

$\wedge$	=	unit vector
$\star$	=	critical
$\cdot$	=	time derivative

Subscript

b	=	back
f	=	final
fr	=	front
n	=	conventional
r	=	radial
θ	=	circumferential
0	=	initial
$\odot$	=	sun
$\male$	=	Mars
$\female$	=	Venus

Received 24 April 2006; revision received 25 September 2006; accepted for publication 26 September 2006.

*Associate Professor, Department of Aerospace Engineering; g.mengali@ing.unipi.it. Member AIAA.
†Research Assistant, Department of Aerospace Engineering, a.quarta@ing.unipi.it; Member AIAA.
‡Assistant Professor, Department of Aerospace and Astronautical Engineering; christian.circi@uniroma1.it.
§Scientist, DLR, German Aerospace Center, Mission Operations Section, 82230 Oberpfaffenhofen, Germany; bernd.dachwald@dlr.de. Member AIAA.

Introduction

SOLAR sails provide unique capabilities for space missions, due to their inherent characteristic of supplying continuous thrust over the mission life. This is a particularly important feature for promoting the feasibility of missions that are not practically accessible via conventional propulsion because of their large ΔV requirements. The striking advances in lightweight deployable

booms, ultralightweight sail films, and small satellite technologies, made in the last few years, are inspiring a growing interest in solar sailing based missions. For example, many of the space exploration missions planned by NASA employ solar sails. Among them, some of the nearer-term projects are the Solar Polar Imager, the L1 Diamond, and the Particle Acceleration Solar Orbiter [1]. In Europe, a similar interest exists and the ESA is promoting a number of solar sail based mission studies such as the GeoSail [2] and the Heliopause Explorer [3].

Significant steps have not only been performed to pursue the ground demonstration of system-level sail technology, but also significant work has been concentrated on developing suitable mathematical models to predict the sail behavior in space. Actually, this is a key requirement as it is often difficult, and in some cases even impossible, to verify the in-space performance of a solar sail through ground testing. Because theoretical models can be validated only with real test data under laboratory conditions, the process of modeling and the identification of uncertainties due to model assumptions need to be closely considered.

The development of suitable mathematical models for estimating the performance of solar sails began long ago. A nonperfectly reflecting sail model, described in [4–6], is widely used for solar sail mission analysis, even if most of the currently available results have been obtained assuming ideal reflection characteristics. The local variation effects of the optical sail properties can also be taken into account through the approach by Rios-Reyes and Scheeres [7]. However, all of the preceding models have the common simplifying characteristic that the optical and mechanical properties of the thin metallized solar sail polymer films are assumed to be constant. To overcome, in part, the preceding limitations, a more realistic mathematical model has been recently proposed that includes the optical solar sail degradation effect due to the sail interaction with the space environment [8]. This degradation effect acts on the sail film's optical coefficients which are assumed to vary with time as a function of the sail film's environmental history, that is, the radiation dose.

The aim of this paper is that of further refining the mathematical solar sail force model by introducing a dependence of the sail material thermo-optical characteristics on both constituent and geometrical factors. More precisely, using experimental data, the optical characteristics of the reflecting material are modeled as a function of the cone angle (the angle between the sun line and the normal to the sail), the sun–sail distance, and the surface roughness. This new model is therefore complementary to that described in [8], the latter being devoted to the effects of degradation on the optical parameters only. This further model refinement allows one to investigate the effects of a variation of the optical characteristics on the mission performance for a flat solar sail and is, therefore, preliminary to a more in-depth study that takes into account three-dimensional effects such as the nonplanar sail shape and/or the billow due to the solar radiation pressure.

The paper is organized as follows. The nonperfectly reflecting model is used to describe the acceleration experienced by a solar sail. However, unlike the conventional model characterized by constant coefficients, the force coefficients of the sail are now assumed to depend on the light incidence angle, the surface roughness, and the sun–sail distance. The mathematical model is then simplified with the support of experimental data. As a result, the main variable affecting the force coefficients is shown to be the light incidence angle. The refined solar sail acceleration model is then used to study the minimum time interplanetary rendezvous problem between circular and coplanar planetary orbits. The problem is solved using an indirect approach and the optimal steering law is approximated through a fourth order polynomial. Finally, a number of optimal trajectories toward Mars and Venus are simulated and a comparison is made with the results obtained by using conventional solar sail acceleration models.

Refined Optical Force Model

The propulsive acceleration of a flat solar sail having mass m and area A can be written as [9]

$$\boldsymbol{a} = \frac{\beta_\sigma}{2}\frac{\mu_\odot}{r^2}\left[b_1\cos\alpha\hat{\boldsymbol{r}} + \left(b_2\cos^2\alpha + b_3\cos\alpha\right)\hat{\boldsymbol{n}}\right] \tag{1}$$

where $r = |\boldsymbol{r}|$ is the sun–sail distance (with $\hat{\boldsymbol{r}} \triangleq \boldsymbol{r}/r$), $\hat{\boldsymbol{n}}$ is in the direction $\hat{\boldsymbol{r}}\cdot\hat{\boldsymbol{n}} > 0$, and $\alpha \in [0, \pi/2]$ is defined as

$$\cos\alpha \triangleq \hat{\boldsymbol{r}}\cdot\hat{\boldsymbol{n}} \tag{2}$$

Finally, $\beta_\sigma \triangleq \sigma^*/\sigma$ where $\sigma \triangleq m/A$ is the sail loading and $\sigma^* = 1.539\ \mathrm{g/m^2}$ is a reference sail loading parameter. Unlike the lightness number, that is, the ratio of the maximum acceleration caused by solar photons on the sailcraft (at a given distance r from the sun) to the corresponding sun's gravitational acceleration, β_σ is a fundamental parameter in that it reflects the limits of the sail technology. Note, in fact, that β_σ is independent of the solar sail optical coefficients. For an in-depth discussion about the differences between β and β_σ the reader is referred to [8].

In Eq. (1), the force coefficients of the sail depend on the (fixed) material's thermo-optical characteristics [9]

$$b_1 \triangleq 1 - \rho s \tag{3}$$

$$b_2 \triangleq 2\rho s \tag{4}$$

$$b_3 \triangleq B_{\mathrm{fr}}\rho(1-s) + (1-\rho)f_\epsilon \tag{5}$$

where f_ϵ is defined as

$$f_\epsilon \triangleq \frac{\epsilon_{\mathrm{fr}}B_{\mathrm{fr}} - \epsilon_b B_b}{\epsilon_{\mathrm{fr}} + \epsilon_b} \tag{6}$$

The optical characteristics of the reflecting material and, therefore, the force coefficients, typically depend on different factors such as the surface roughness and the light incidence angle (the latter coincides with the cone angle for a flat reflector). A simplified optical model was developed in the 1970s at the Jet Propulsion Laboratory for a rendezvous mission to Halley's comet [10,11]. In that model, all of the force coefficients take constant values $b_1 = b_{1n}$, $b_2 = b_{2n}$, and $b_3 = b_{3n}$, and depend on the (fixed) material's thermo-optical characteristics only. This model will be referred to as the conventional or nominal optical force model to distinguish it from the refined model that will be discussed later.

Consider a reference solar sail film with a highly reflecting front side of aluminum and a highly emissive back side of chromium. As it is shown by Eqs. (3–5), the specular reflectance of the reflecting film plays a central role in establishing the sailcraft acceleration and performance. The reflectance, in turn, depends on the light incidence angle (or the cone angle) and on the roughness of the surface finish. The roughness quantifies the number of microirregularities with a certain height distribution (in terms of hills and valleys with respect to a mean surface level) and a spatial separation. Using the scalar scattering theory [12], it is possible to express the coefficients ρ and s through the following functional representation

$$\rho = \rho(\alpha); \qquad s = s(\alpha, h) \tag{7}$$

Figures 1 and 2 and Table 1 illustrate the numerical values of ρ and s for the reference sail. The numerical data have been experimentally obtained by Vulpetti and Scaglione [12] for the Aurora project [13] using unpolarized solar light (but polarization arises upon reflection) and a solar spectrum ranging, in wavelength, from 2800 to 40,000 Å. The interested reader is referred to [12] for a detailed discussion as to how the experimental data were obtained.

Note that $h = 0$ should be thought of as a limit case where the roughness is zero and the photons which are not absorbed are specularly reflected [that is, $s(\alpha, h = 0) \equiv 1$]. However, this case is different from the ideal case because a fraction of the incident photons is absorbed by the sail [$\rho(\alpha) < 1$]. In the ideal model,

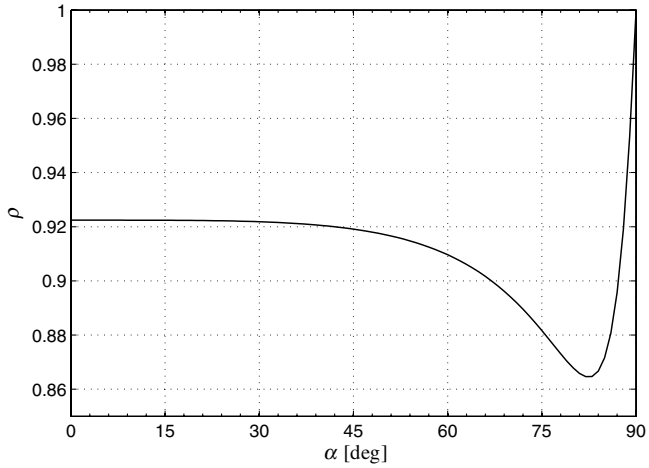

Fig. 1 Reflection coefficient as a function of the cone angle.

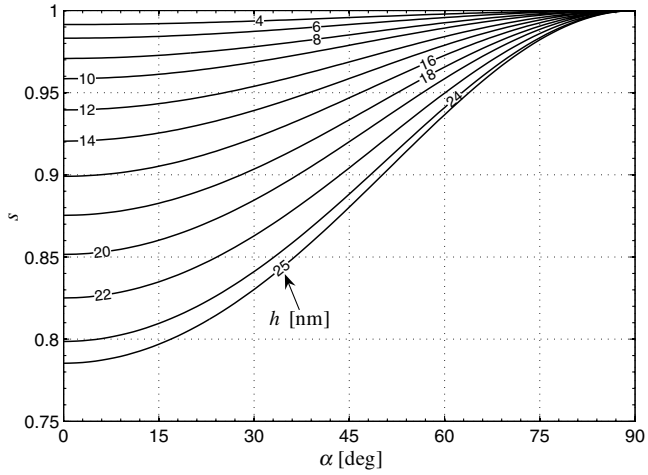

Fig. 2 Fraction of specularly reflected photons as a function of α and h.

instead, all of the incident photons are specularly reflected [$\rho(\alpha) \equiv 1$].

The emissivity coefficient can be expressed as a function of the sail equilibrium temperature through a best-fit second order polynomial expression having semi-experimental origin [14–16]:

$$\epsilon = c_0 + c_1(T - \tilde{T}) + c_2(T - \tilde{T})^2 \tag{8}$$

Both the various c_i and $\tilde{T}$ depend on the material employed.

Assuming the aluminum melting temperature as the temperature unit (TeU), that is TeU $\triangleq$ 933 K, Table 2 shows the numerical values of the coefficients involved in Eq. (8) for aluminum and chromium. The functions $\epsilon_{\rm fr} = \epsilon_{\rm fr}(T)$ and $\epsilon_b = \epsilon_b(T)$, obtained from Eq. (8), are illustrated in Figs. 3a and 3b for the reference sail.

The equilibrium temperature can be calculated as a function of the cone angle and the sun–sail distance, using the power balance between the thermal input and thermal output (see [6], p. 49). The result is

$$T = \left(\frac{(1-\rho) c P_\oplus r_\oplus^2 \cos\alpha}{r^2 \tilde{\sigma} (\epsilon_{\rm fr} + \epsilon_b)} \right)^{1/4} \tag{9}$$

where $\tilde{\sigma} = 5.67051 \times 10^{-8}$ W/m^2/K^4, $r_\oplus \triangleq 1$ AU, and $P_\oplus = 4.5632$ N/km^2 is the solar radiation pressure at $r_\oplus$.

Substituting Eq. (8) into Eq. (9), the following polynomial equation of order 6 in the variable T is obtained

$$d_6 T^6 + d_5 T^5 + d_4 T^4 = d_0 \tag{10}$$

where

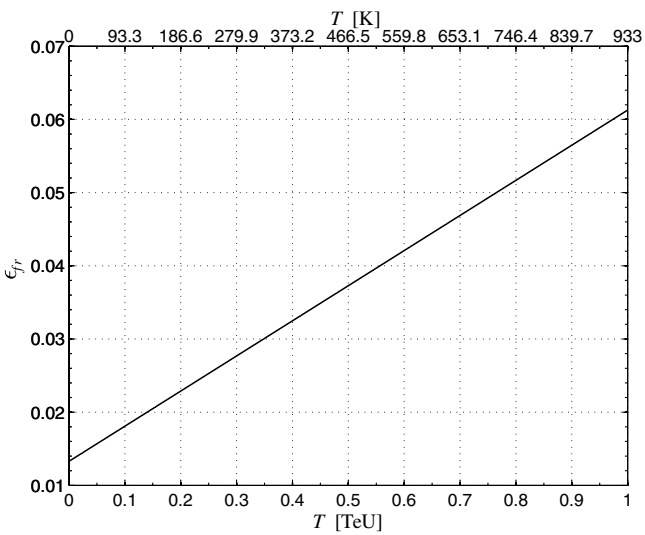

a) Front surface emissivity (aluminium)

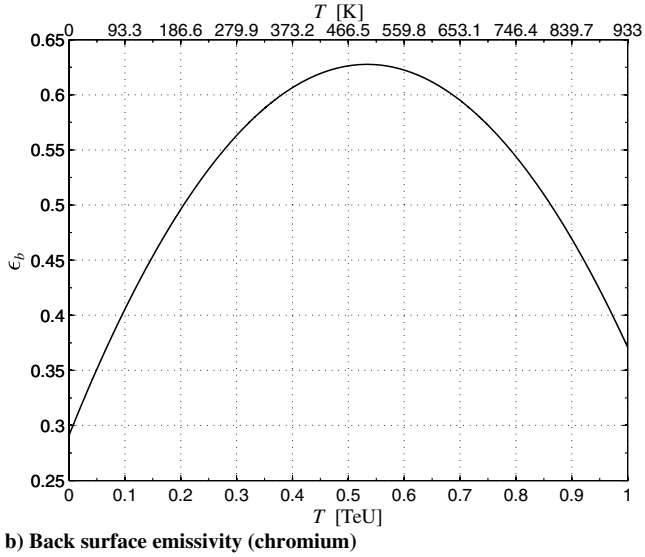

b) Back surface emissivity (chromium)

Fig. 3 Front and back emissivities as functions of T for the reference sail surface.

$$d_6 \triangleq c_{2_b} + c_{2_{\rm fr}} \tag{11}$$

$$d_5 \triangleq c_{1_{\rm fr}} + c_{1_b} - 2\tilde{T}_b c_{2_b} - 2\tilde{T}_{\rm fr} c_{2_{\rm fr}} \tag{12}$$

$$d_4 \triangleq c_{2_{\rm fr}} \tilde{T}_{\rm fr}^2 + c_{2_b} \tilde{T}_b^2 - c_{1_{\rm fr}} \tilde{T}_{\rm fr} - c_{1_b} \tilde{T}_b + c_{0_{\rm fr}} + c_{0_b} \tag{13}$$

$$d_0 \triangleq \frac{(1-\rho) c P_\oplus r_\oplus^2 \cos\alpha}{r^2 \tilde{\sigma}} \tag{14}$$

Once the sail coating materials are chosen (and, therefore, the coefficients d_4, d_5, and d_6 are known) the solution of Eq. (10) gives the equilibrium temperature as a function of the parameter d_0 that depends on the cone angle and on the distance from the sun r [see Eq. (14)]. Because for a given pair (α, r) Eq. (10) has six roots, one may wonder whether there is an ambiguity in finding the correct value of T. To answer this question one should recall that in Eq. (10) d_0 is the only coefficient that varies as the cone angle and/or the solar distance changes. Therefore, Eq. (10) can be easily translated into a classical Evans's root locus form in which d_0 is treated as a nonnegative parameter. The result is shown in Fig. 4 where the six branches of the locus correspond to the solutions of Eq. (10) for

Table 1 Sail optical characteristics as a function of cone angle and surface roughness

α	ρ	s, %				
deg	%	$h = 5$ nm	$h = 10$ nm	$h = 15$ nm	$h = 20$ nm	$h = 25$ nm
0	92.24	98.93	95.85	91.1	85.16	78.53
2	92.24	98.93	95.85	91.11	85.17	78.55
4	92.24	98.94	95.87	91.14	85.22	78.62
6	92.24	98.94	95.89	91.19	85.3	78.72
8	92.24	98.95	95.93	91.26	85.41	78.86
10	92.24	98.96	95.97	91.35	85.54	79.05
12	92.24	98.98	96.02	91.45	85.71	79.28
14	92.24	98.99	96.08	91.58	85.91	79.54
16	92.24	99.01	96.15	91.72	86.14	79.85
18	92.23	99.03	96.23	91.88	86.39	80.19
20	92.23	99.06	96.32	92.06	86.67	80.57
22	92.23	99.08	96.41	92.26	86.98	80.99
24	92.22	99.11	96.51	92.47	87.32	81.45
26	92.21	99.13	96.62	92.69	87.67	81.94
28	92.2	99.16	96.74	92.93	88.06	82.47
30	92.18	99.2	96.86	93.18	88.46	83.02
32	92.17	99.23	96.98	93.44	88.88	83.61
34	92.14	99.26	97.11	93.72	89.33	84.23
36	92.12	99.3	97.25	94	89.79	84.87
38	92.08	99.33	97.38	94.29	90.26	85.54
40	92.05	99.37	97.52	94.59	90.75	86.23
42	92	99.41	97.67	94.89	91.25	86.94
44	91.94	99.44	97.81	95.2	91.76	87.67
46	91.88	99.48	97.96	95.51	92.27	88.41
48	91.8	99.52	98.1	95.82	92.79	89.16
50	91.71	99.56	98.24	96.13	93.31	89.91
52	91.6	99.59	98.39	96.44	93.83	90.67
54	91.48	99.63	98.53	96.75	94.35	91.43
56	91.33	99.66	98.67	97.05	94.86	92.18
58	91.16	99.7	98.8	97.34	95.36	92.93
60	90.97	99.73	98.93	97.62	95.85	93.66
62	90.74	99.76	99.06	97.9	96.32	94.37
64	90.47	99.79	99.18	98.16	96.78	95.05
66	90.17	99.82	99.29	98.42	97.21	95.71
68	89.81	99.85	99.4	98.65	97.63	96.34
70	89.41	99.87	99.5	98.87	98.01	96.93
72	88.95	99.9	99.59	99.08	98.37	97.48
74	88.44	99.92	99.67	99.26	98.7	97.98
76	87.88	99.94	99.75	99.43	98.99	98.44
78	87.31	99.95	99.81	99.58	99.25	98.84
80	86.79	99.97	99.87	99.7	99.48	99.18
82	86.46	99.98	99.92	99.81	99.66	99.47
84	86.67	99.99	99.95	99.89	99.81	99.7
86	88.07	99.99	99.98	99.95	99.91	99.87
88	91.91	100	99.99	99.99	99.98	99.97
90	100	100	100	100	100	100

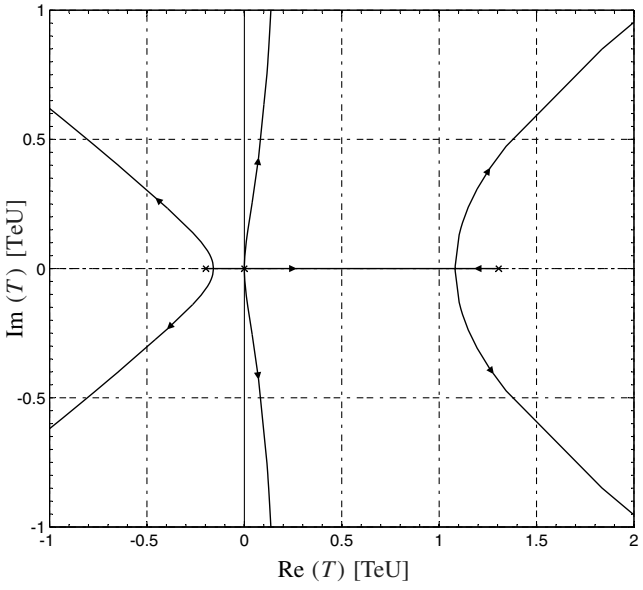

Fig. 4 Root locus of Eq. (10) as a function of the parameter d_0.

different values of d_0. Figure 4 shows that for a certain range of variation of d_0 there are two real positive solutions of Eq. (10). However, one only is physically acceptable, the other being greater than the aluminum melting temperature ($T > 1$ TeU). Using the values in Table 2 and the dependence of the reflection coefficient on the cone angle (see Table 1), the equilibrium temperature of the reference sail can be obtained as a function of α and r. The results are plotted in Fig. 5.

From Fig. 5, one concludes that if the sun–sail distance is constrained to be greater than a minimum admissible value $r_{\min} = 0.3$ AU [17], the corresponding solar sail maximum temperature does not exceed 470 K. This value is below $T_{\lim} = 513$ K $= 0.5498$ TeU, which is the limit working temper-

Table 2 Coefficients of the polynomial approximation for the reference sail, see Eq. (8)

	c_0	c_1	c_2	$\tilde{T}$
		TeU^{-1}	TeU^{-2}	TeU
Aluminium	0.039	0.047983	0	0.53591
Chromium	0.62	−0.18968	−1.1807	0.61415

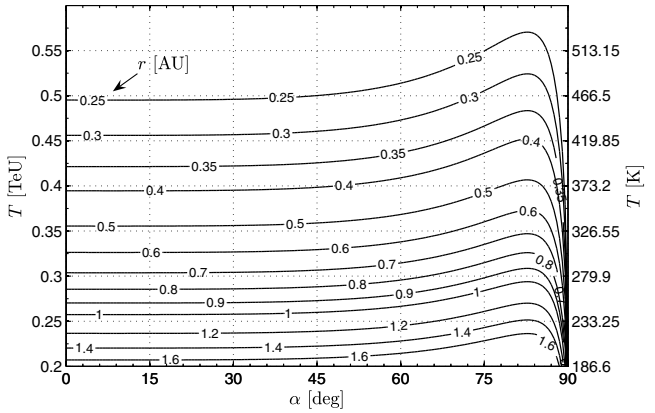

Fig. 5 Sail equilibrium temperature as a function of α and r.

ature typically used for the reference sail (see [17,18]). Note, however, that a translation of the sail temperature limits into constraints concerning the sail film materials is beyond the scope of this paper because the maximum allowed sail film temperature depends not only on the film material, but also on the sail design (stresses, wrinkles, etc.).

Figure 5 also shows an increase in the temperature for high values of the cone angle. This behavior is closely related to the dependence of the temperature on ρ [see Eq. (9)]. The latter, in turn, depends on the cone angle as is shown in Fig. 1 (in particular, note that the minimum value of ρ in Fig. 1 is closely connected to the maximum value of T in Fig. 5).

Figure 6 shows the emissivity coefficients as a function of the cone angle and the sun–sail distance. It is interesting to investigate the influence that α, r, and h have on the force coefficients. Note that only

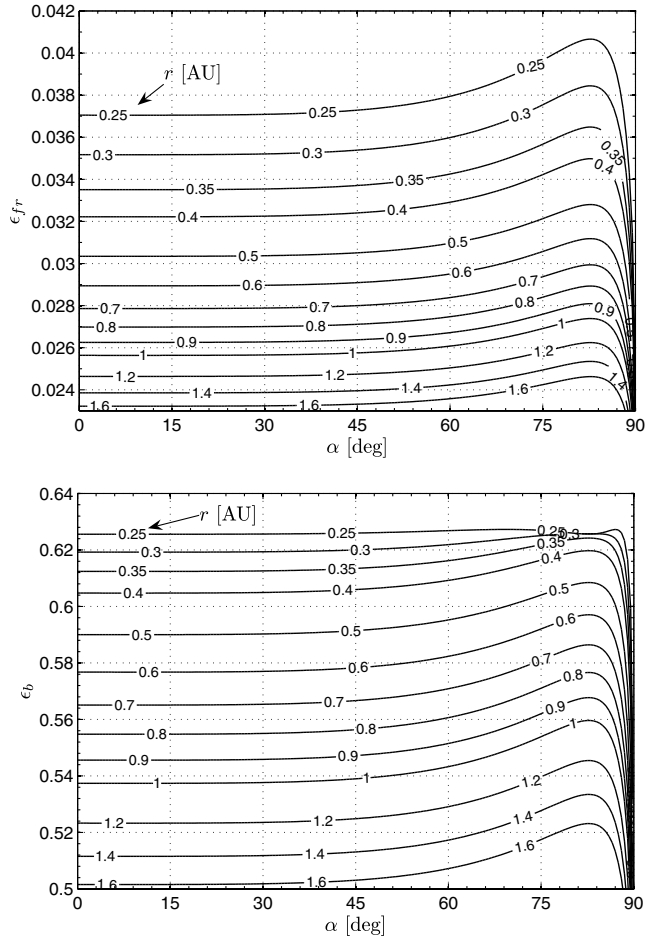

Fig. 6 Front and back emissivities as functions of α and r.

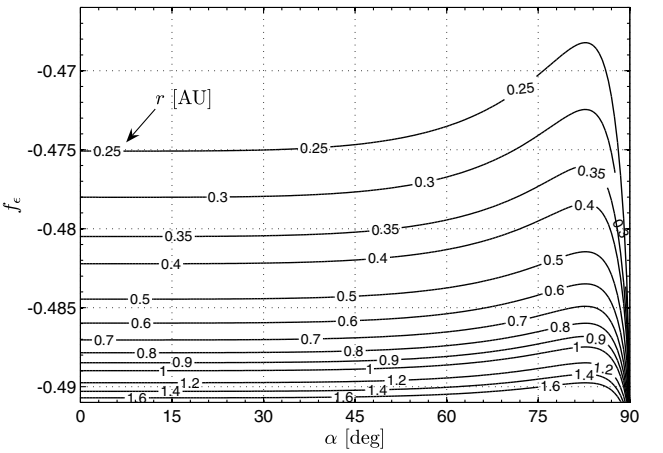

Fig. 7 Function $f_\epsilon = f_\epsilon(\alpha, r)$ for the reference sail, see Eq. (6).

b_3, given by Eq. (5), depends on the sun–sail distance through the emissivities [see Eq. (8)]. The dependence of b_3 on r can be studied through the function $f_\epsilon = f_\epsilon(\alpha, r)$ defined in Eq. (6). Assuming [5] $B_{\rm fr} = 0.79$ (for aluminum), and $B_b = 0.55$ (for chromium), Fig. 7 shows the function f_ϵ. Note that f_ϵ is approximately independent of the sun–sail distance and so is the force coefficient b_3. Indeed

$$\left|\frac{f_\epsilon(\alpha, r) - f_\epsilon(\alpha, r_\oplus)}{f_\epsilon(\alpha, r_\oplus)}\right| \leq 3\% \quad \text{for } r \in [0.3, 5.2] \text{ AU} \tag{15}$$

Therefore, during an interplanetary mission, the value of b_3 is roughly independent of r and equal to the value calculated at the departure, or $b_3(\alpha, h, r) \simeq b_3(\alpha, h, r_\oplus) \triangleq b_{3_\oplus}(\alpha, h)$. This assumption remarkably simplifies the calculation of the solar sail propulsive acceleration. In fact, having estimated the initial roughness of the sail, the latter can be considered, with good approximation, to be constant during the whole mission. As a result, the generic sail force coefficient b_i, and hence the acceleration given by Eq. (1), is an implicit function of the cone angle only. Figure 8 shows the

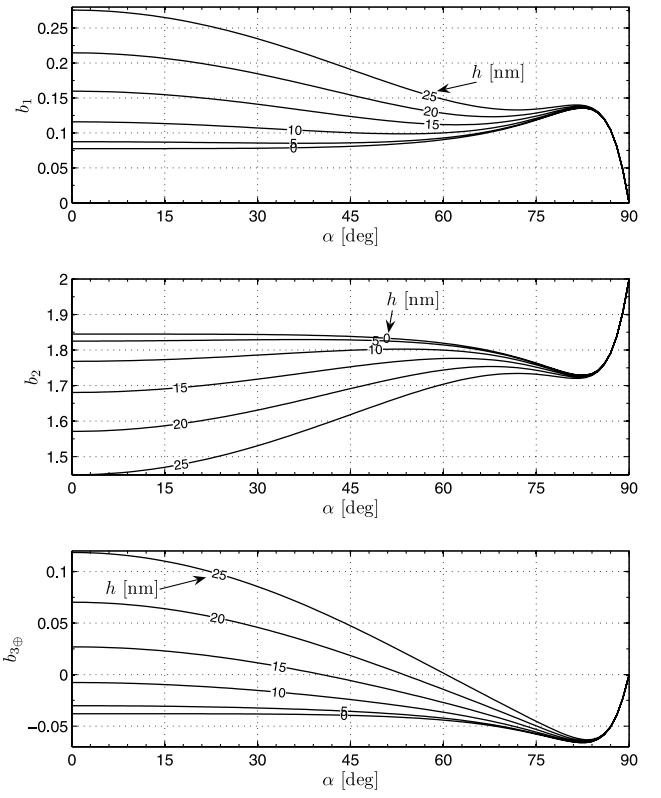

Fig. 8 Force coefficients as functions of α and h.

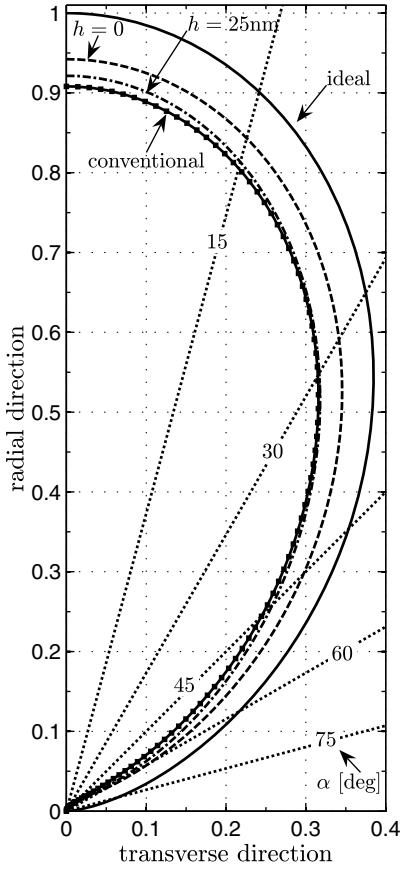

Fig. 9 Shape of α-bubble. The constant α-lines refer to the ideal force model.

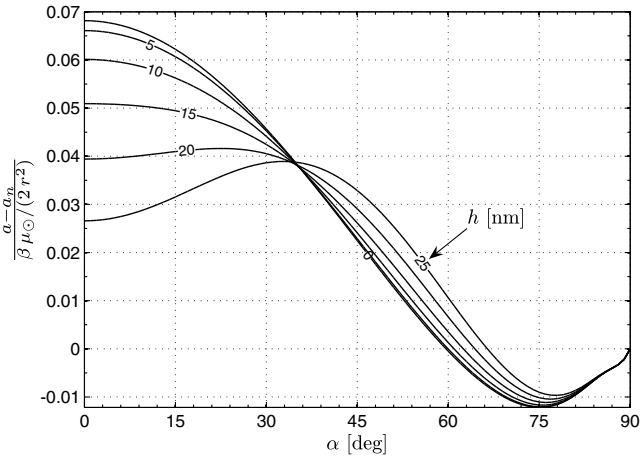

Fig. 10 Comparison between sail accelerations for the refined and conventional optical force model.

dependence of b_1, b_2, and $b_{3_\oplus}$ on α and h. Note that the values of the force coefficients are different from the constant values ($b_{1n} = 0.1728$, $b_{2n} = 1.6544$, and $b_{3n} = -0.00109$) that are usually taken for the conventional optical force model (see [5]).

Figure 9 illustrates the shape of the $\boldsymbol{a}$-bubble, that is the bubble on which surface the tip of the vector $\boldsymbol{a}$, defined by Eq. (1), is constrained to lie. The dependence of the force coefficient on α and h produces a variation in the shape of the $\boldsymbol{a}$-bubble with respect to both the ideal case of specular reflection and to the conventional optical case (scales are normalized with the maximum ideal acceleration value $a_{\max} = \beta_\sigma \mu_\odot / r^2$). The dimensionless projection of the solar sail acceleration is illustrated in Fig. 9 in the radial (parallel to $\hat{\boldsymbol{r}}$) and transverse (normal to $\hat{\boldsymbol{r}}$) direction. The sail acceleration corresponding to the refined optical model with $h = 25$ nm exceeds a little the acceleration obtained with the conventional optical model a_n. The resemblance between the optical model with $h = 25$ nm and the conventional one is at the base of the similarities in the mission times found in the simulations, as discussed later. Nevertheless, note that for a given value of α, the modulus of the acceleration is different from the conventional case. This behavior is clearly shown in Fig. 10 in which the difference $a - a_n$ is shown in dimensionless form. Note that for cone angles higher than about 60 deg, the conventional model seems to provide better performance. Actually, as previously discussed, the performance of the conventional model is always less than that of the refined model, at least as long as the variation of the surface roughness is in the range shown in Fig. 9.

Minimum Time Rendezvous

To better appreciate the differences between the refined force model with respect to the conventional one, a comparison has been established through the analysis of a circle-to-circle interplanetary rendezvous problem between coplanar orbits.

The heliocentric equations of motion for a spacecraft in a polar inertial frame $\mathcal{T}_\odot(r, \theta)$ are

$$\dot{r} = u \tag{16}$$

$$\dot{\theta} = \frac{v}{r} \tag{17}$$

$$\dot{u} = \frac{v^2}{r} - \frac{\mu_\odot}{r^2} + a_r \tag{18}$$

$$\dot{v} = -\frac{uv}{r} + a_\theta \tag{19}$$

where the polar angle is measured counterclockwise from some reference position. The cone angle is measured counterclockwise from the radial direction. In Eqs. (18) and (19), the terms a_r and a_θ denote radial and circumferential sailcraft accelerations. Recalling Eq. (2), from Eq. (1) one obtains

$$a_r = \frac{\beta_\sigma}{2}\frac{\mu_\odot}{r^2}\cos\alpha[b_1 + \cos\alpha(b_2\cos\alpha + b_3)] \tag{20}$$

$$a_\theta = \frac{\beta_\sigma}{2}\frac{\mu_\odot}{r^2}\sin\alpha\cos\alpha(b_2\cos\alpha + b_3) \tag{21}$$

The problem is to minimize the time necessary to transfer the spacecraft from the Earth's heliocentric orbit of radius $r_\oplus$ to the target planet circular orbit $r(t_f) = r_f$. This amounts to maximizing the performance index

$$J = -t_f \tag{22}$$

The problem is now solved using an indirect approach. The Hamiltonian of the system is given by

$$H = \lambda_r u + \lambda_\theta \frac{v}{r} + \lambda_u\left(\frac{v^2}{r} - \frac{\mu}{r^2} + a_r\right) + \lambda_v\left(-\frac{uv}{r} + a_\theta\right) \tag{23}$$

where the adjoint variables are associated with the state variables. The time derivatives of the adjoint variables are given by the Euler–Lagrange equations, that is

$$\dot{\lambda}_r = \frac{\lambda_\theta v}{r^2} + \lambda_u\left(\frac{v^2}{r^2} - \frac{2\mu}{r^3} - \frac{\partial a_r}{\partial r}\right) - \lambda_v\left(\frac{uv}{r^2} + \frac{\partial a_\theta}{\partial r}\right) \tag{24}$$

$$\dot{\lambda}_\theta = 0 \tag{25}$$

$$\dot{\lambda}_u = -\lambda_r + \lambda_v \frac{v}{r} \tag{26}$$

$$\dot{\lambda}_v = -\frac{\lambda_\theta}{r} - 2\frac{\lambda_u v}{r} + \frac{\lambda_v u}{r} \tag{27}$$

Under the previously discussed assumption $b_3 \simeq b_{3_\oplus}$ (the dependence of b_3 on r is neglected), the partial derivatives of the acceleration in Eq. (24) are given by

$$\left[\frac{\partial a_r}{\partial r}, \frac{\partial a_\theta}{\partial r}\right]^T = -\frac{2}{r}[a_r, a_\theta]^T \tag{28}$$

The differential problem is completed by the boundary conditions at the initial time $t = t_0 = 0$ and at the final time $t = t_f$, that is

$$r(t_0) = r_\oplus, \qquad \theta(t_0) = u(t_0) = 0, \qquad v(t_0) = \sqrt{\mu_\odot / r_\oplus} \tag{29}$$

$$r(t_f) = r_f, \qquad \lambda_\theta(t_f) = u(t_f) = 0, \qquad v(t_f) = \sqrt{\mu_\odot / r_f} \tag{30}$$

The optimal mission time is obtained by enforcing the transversality condition [19] $H(t_f) = 1$.

Optimal Steering Law

From Pontryagin's maximum principle, the optimal steering law $\alpha(t)$ must maximize H at any time. This amounts to maximizing that portion H' of the Hamiltonian that explicitly depends on the control vector, that is

$$\alpha = \arg \max_\alpha H \equiv \arg \max_\alpha H' \tag{31}$$

where

$$H' \triangleq \lambda_u a_r + \lambda_v a_\theta = \sqrt{\lambda_u^2 + \lambda_v^2}(a_r \cos\alpha_\lambda + a_\theta \sin\alpha_\lambda) \tag{32}$$

In Eq. (32), α_λ is the angle between the primer vector [20] $[\boldsymbol{\lambda}_v]_{\mathcal{T}_\odot} \triangleq [\lambda_u, \lambda_v]^T$ and $\hat{\boldsymbol{r}}$. One has

$$\cos\alpha_\lambda = \frac{\lambda_u}{\sqrt{\lambda_u^2 + \lambda_v^2}}, \qquad \sin\alpha_\lambda = \frac{\lambda_v}{\sqrt{\lambda_u^2 + \lambda_v^2}} \tag{33}$$

When Eqs. (20) and (21) are substituted into Eq. (32), the optimal control law is found by maximizing $\tilde{H}'$ with respect to α, where

$$\tilde{H}' \triangleq \cos\alpha(b_2 \cos\alpha + b_3)(\sin\alpha_\lambda \sin\alpha + \cos\alpha_\lambda \cos\alpha) + b_1 \cos\alpha_\lambda \cos\alpha \tag{34}$$

The expression $\alpha = \alpha(\alpha_\lambda)$ which maximizes $\tilde{H}'$ in the ideal case ($b_1 = b_3 = 0$ and $b_2 = 2$) has been found analytically by Sauer in [21]. The conventional case ($b_i = b_{\text{in}}$, $i = 1, 2, 3$) has been studied by Mengali and Quarta [9] who proposed a semi-analytical solution.

Assuming a refined optical model with $b_3 = b_{3_\oplus}$, the function $\tilde{H}'$ depends in implicit form on h and α. However, because we know the numerical (and not the analytical) dependence of the force coefficients on the cone angle, the maximization of $\tilde{H}'$ with respect to α can be obtained in numerical form only, provided that the surface roughness of the material is given. An example of the function $\alpha = \alpha(\alpha_\lambda)$ is illustrated in Fig. 11. Figure 11 shows that the function $\alpha = \alpha(\alpha_\lambda)$ has a discontinuity for $\alpha_\lambda = \alpha_\lambda^\star \cong 150$ deg. The reason is that when $\alpha_\lambda > \alpha_\lambda^\star$ the stationarity of Eq. (32) is satisfied by pairs (α_λ, α) that render $\tilde{H}' < 0$. As a result, when $\alpha_\lambda > \alpha_\lambda^\star$, the maximum value for the modified Hamiltonian equation is obtained by setting $\tilde{H}' = 0$. The corresponding value of the cone angle is $\alpha = \pi/2$ [see Eq. (34)]. This result agrees with a similar behavior previously found for the conventional optical force model [9].

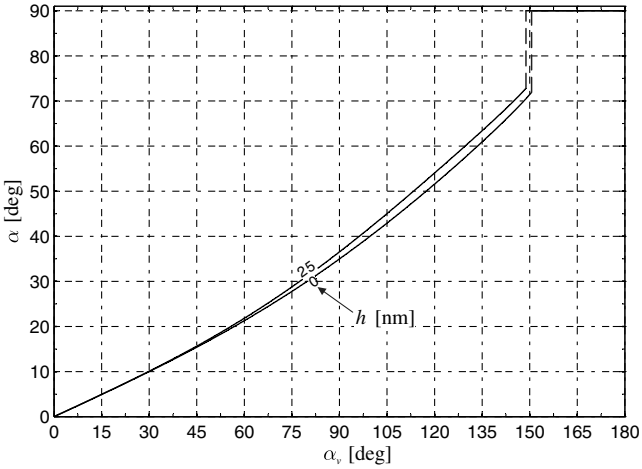

Fig. 11 Optimal control law for refined optical force model ($b_3 = b_{3_\oplus}$) with $h = (0, 25)$ nm.

Once the numerical solution of the optimal control law is found, the latter can be analytically treated through a least square polynomial approximation to reduce the calculation volume necessary to perform the simulations. Accurate results have been obtained using the following approximation

$$\alpha = \begin{cases} e_4\alpha_\lambda^4 + e_3\alpha_\lambda^3 + e_2\alpha_\lambda^2 + e_1\alpha_\lambda & \text{if } \alpha_\lambda \le \alpha_\lambda^\star \\ \pi/2 & \text{if } \alpha_\lambda > \alpha_\lambda^\star \end{cases} \tag{35}$$

where the generic coefficient and the critical angle depend on the surface roughness. The results obtained for different values of h have been summarized in Table 3.

Note that Eq. (35) is valid also for three-dimensional transfers. In fact, the problem of maximizing the Hamiltonian with respect to α in a three-dimensional framework can be easily translated [9] into the problem of maximizing $\tilde{H}'$. Therefore, the optimal steering law coincides with that shown in Fig. 11 and is approximated by Eq. (35).

Case Study

The previously discussed control law has been used to study the minimum time rendezvous mission toward Mars ($r_f \equiv r_{\mathcal{O}^\prime} = 1.5237$ AU) and Venus ($r_f \equiv r_{\mathcal{Q}} = 0.7233$ AU).

A number of trajectories have been simulated with values of the dimensionless sail loading parameter ranging in the interval $\beta_\sigma \in$

Table 3 Coefficients of the polynomial approximation of the optimal control law, see Eq. (35)

h	e_4	e_3	e_2	e_1	$\alpha_\lambda^\star$
nm	rad^{-3}	rad^{-2}	rad^{-1}		rad
0	−0.004219	0.03378	−0.002663	0.3258	2.6285
5	−0.004434	0.03443	−0.002601	0.3258	2.6285
10	−0.005292	0.03735	−0.003845	0.3262	2.6232
15	−0.006647	0.04194	−0.00565	0.3266	2.6180
20	−0.008658	0.04907	−0.009565	0.3278	2.6075
25	−0.01099	0.05717	−0.01331	0.3283	2.5970
Conventional	0.001404	0.01759	0.01761	0.3142	2.5468

Table 4 Flight times for Earth–Mars circle-to-circle rendezvous using refined optical force model

β_σ	Flight time t_f, days				
	Ideal	Conventional	$h = 0$ nm	$h = 10$ nm	$h = 25$ nm
1	239	270	256	257	265
0.95	242	273	259	260	268
0.9	246	276	262	264	271
0.85	249	280	266	267	275
0.8	253	284	270	271	279
0.75	258	288	274	276	283
0.7	262	293	279	280	288
0.65	268	298	284	286	294
0.6	274	304	290	292	300
0.55	280	311	297	299	307
0.5	288	319	305	306	315
0.45	297	328	314	315	324
0.4	308	339	324	326	335
0.35	320	352	337	339	349
0.3	336	369	353	355	365
0.25	356	391	374	377	387
0.24	361	396	379	382	392
0.23	366	401	385	387	398
0.22	372	407	390	393	404
0.21	377	414	397	399	410
0.2	384	421	403	406	417
0.19	391	428	410	413	425
0.18	398	437	418	421	433
0.17	406	446	427	430	442
0.16	415	456	437	440	453
0.15	426	468	448	450	464
0.14	437	481	460	463	478
0.13	450	496	474	477	493
0.12	465	515	490	494	512
0.11	483	540	511	515	537
0.1	505	578	538	544	574
0.09	535	704	585	597	689
0.08	591	803	733	746	796
0.07	751	882	827	836	876
0.06	850	970	915	923	964
0.05	954	1119	1027	1039	1109
0.045	1023	1301	1144	1173	1289
0.04	1162	1427	1331	1348	1418
0.035	1356	1575	1467	1483	1566
0.03	1515	1879	1703	1740	1867
0.025	1850	2212	2014	2039	2192
0.02	2281	2756	2508	2540	2732

Table 5 Flight times for Earth–Venus circle-to-circle rendezvous using refined optical force model

β_σ	Flight time t_f, days				
	Ideal	Conventional	$h = 0$ nm	$h = 10$ nm	$h = 25$ nm
1	121	137	130	130	134
0.95	122	138	131	132	135
0.9	124	140	133	133	137
0.85	126	142	134	135	139
0.8	128	144	136	137	141
0.75	130	146	139	139	143
0.7	132	148	141	142	146
0.65	135	151	144	145	149
0.6	138	154	147	148	152
0.55	141	157	150	151	155
0.5	145	161	154	155	159
0.45	150	166	159	160	164
0.4	155	171	164	165	169
0.35	161	178	170	171	176
0.3	169	186	178	179	184
0.25	179	197	189	190	195
0.24	181	199	191	192	197
0.23	184	202	194	195	200
0.22	187	205	196	198	203
0.21	190	208	199	201	206
0.2	193	211	203	204	209
0.19	196	215	206	207	213
0.18	200	219	210	211	217
0.17	204	223	214	215	221
0.16	208	228	219	220	226
0.15	213	233	224	225	231
0.14	218	239	229	231	237
0.13	224	246	236	237	244
0.12	231	254	243	244	252
0.11	239	263	251	253	261
0.1	248	274	262	263	272
0.09	260	288	274	276	287
0.08	274	311	292	294	309
0.07	295	392	323	330	383
0.06	351	462	427	433	458
0.05	453	519	490	495	516
0.045	488	554	523	528	551
0.04	525	604	562	568	600
0.035	571	727	636	652	720
0.03	687	819	768	776	815
0.025	808	979	876	889	969
0.02	1009	1194	1106	1119	1186

$[0.02, 1]$ and three different values of the surface roughness $h \in (0, 10, 25)$ nm. The chosen values of β_σ correspond to sail characteristic accelerations (defined as the maximum propelling sail acceleration for an ideal sail at 1 AU) ranging in the interval $a_c \in [0.12, 5.93]$ mm/s^2.

The simulation results are shown in Tables 4 and 5. To better emphasize a comparison with the available sail force models, the tables include the transfer times for the ideal sail model [21] and the conventional optical model [9].

Tables 4 and 5 show that, as expected, the sail performance decreases as the value of the surface roughness is increased. For example, considering an Earth–Mars rendezvous, the transfer time for $h = 0$ ($h = 25$ nm) is less than about 10% (1%) with respect to the conventional case for small values of β_σ, whereas it is about 5% (2%) for high values of β_σ. Also, the difference in terms of transfer times between the refined, conventional, and ideal models appears to be inversely proportional to the value of β_σ. This result is in accordance with a similar trend pointed out by Dachwald using the conventional force model [22].

We finally note that the surface roughness affects substantially the time history of the sail control angle α, as is clearly shown in Fig. 12. Note the close similarity between the time histories of the conventional model and that with $h = 25$ nm. This agrees with the previously discussed resemblance between the $\boldsymbol{a}$-bubble for the two models.

Conclusions

A refined mathematical model for the description of the acceleration experienced by a flat solar sail has been introduced and discussed. The new model is able to capture the dependence of the solar sail force coefficients on the light incidence angle, the surface

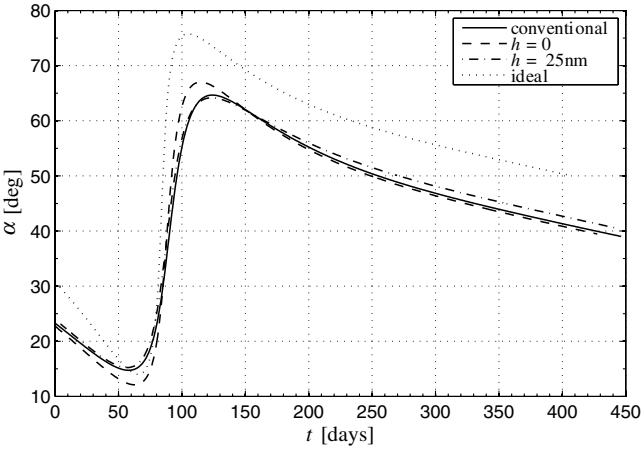

Fig. 12 Earth–Mars transfer with $\beta_\sigma = 0.17$ for different solar sail force models (time history).

roughness, and the sun–sail distance. Using the support of experimental data, we have shown that the main variable affecting the force coefficients is the light incidence angle that, for a flat sail, coincides with the cone angle. As a result, for a given value of the cone angle, the acceleration modulus is different from the value that would be estimated with the conventional model. The impact of these differences over the mission times have been quantified by studying the minimum time interplanetary rendezvous problem between circular and coplanar planetary orbits. The problem has been solved using an indirect approach and the optimal steering law has been approximated in polynomial form. Although the case studies refer to planar transfer problems, the same steering law is valid for three-dimensional transfers, as well. A number of optimal trajectories toward Mars and Venus have been simulated for different values of the dimensionless sail loading parameter and of the surface roughness. The sail loading parameter is responsible for percentage differences in mission times up to 5–10% with respect to the conventional model, whereas the roughness is shown to affect significantly the time history of the optimal steering law. Although three-dimensional effects, such as the nonplanar sail shape and the billow due to the solar radiation pressure have not been taken into account, the new model provides a more realistic description of a solar sail behavior.

Acknowledgments

The research of the first two authors has been financed, in part, by the Italian Ministry of Education, University, and Research. The authors are indebted to Giovanni Vulpetti for providing the experimental data from the Aurora Project.

References

[1] Montgomery, E. E., and Johnson, L., "Development of Solar Sail Propulsion for NASA Science Missions to the Inner Solar System," *45th AIAA/ASME/ASCE/AHS/ASC Structures, Structural Dynamics and Materials Conference*, AIAA Paper 2004-1506, Palm Springs, CA, 19–22 April 2004.

[2] Macdonald, M., McInnes, C. R., Alexander, D., and Sandman, A., "GeoSail: Exploring the Magnetosphere Using a Low-Cost Solar Sail," *Acta Astronautica*, Vol. 59, Nos. 8–11, Oct.–Dec. 2006, pp. 757–767.

[3] Leipold, M., Fichtner, H., Heber, B., Groepper, P., Lascar, S., Burger, F., Eiden, M., Niederstadt, T., Sickinger, C., Herbeck, L., Dachwald, B., and Seboldt, W., "Heliopause Explorer: A Sailcraft Mission to the Outer Boundaries of the Solar System,"*Acta Astronautica*, Vol. 59, Nos. 8–11, Oct.–Dec. 2006, pp. 785–796.

[4] Forward, R., "Grey Solar Sails," *Journal of the Astronautical Sciences*, Vol. 38, No. 2, 1990, pp. 161–185.

[5] Wright, J. L., *Space Sailing*, Gordon and Breach, Berlin, 1992, pp. 227–233.

[6] McInnes, C. R., *Solar Sailing: Technology, Dynamics and Mission Applications*, Springer–Praxis Series in Space Science and Technology, Springer–Verlag, Berlin, 1999, pp. 46–54.

[7] Rios-Reyes, L., and Scheeres, D., "Generalized Model for Solar Sails," *Journal of Spacecraft and Rockets*, Vol. 42, No. 1, 2005, pp. 182–185.

[8] Dachwald, B., Mengali, G., Quarta, A. A., and Macdonald, M., "Parametric Model and Optimal Control of Solar Sails with Optical Degradation," *Journal of Guidance, Control, and Dynamics*, Vol. 29, No. 5, Sept.–Oct. 2006, pp. 1170–1178.

[9] Mengali, G., and Quarta, A. A., "Optimal Three-Dimensional Interplanetary Rendezvous Using Nonideal Solar Sail," *Journal of Guidance, Control, and Dynamics*, Vol. 28, No. 1, Jan.–Feb. 2005, pp. 173–177.

[10] Sauer, C. G., Jr., "Comparison of Solar Sail and Ion Drive Trajectories for a Halley's Comet Rendezvous Mission," American Astronautical Society Paper 77-104, Sept. 1977.

[11] Wood, L. J., "Navigation Accuracy Analysis for a Halley Intercept Mission," *Journal of Guidance, Control, and Dynamics*, Vol. 5, No. 3, May–June 1982, pp. 300–306.

[12] Vulpetti, G., and Scaglione, S., "Aurora Project: Estimation of the Optical Sail Parameters," *Acta Astronautica*, Vol. 44, Nos. 2–4, Jan.–Feb. 1999, pp. 123–132.

[13] Vulpetti, G., "AURORA Project: Flight Design of a Technology Demonstration Mission," *IAA Symposium on Realistic Near-Term Advanced Scientific Space Missions*, International Academy of Astronautics Paper 96-T-2.01, Torino, Italy, June 1996.

[14] Vulpetti, G., "Overview of Advanced Space Propulsion Via Solar Photon Sailing," Scuola di Ingegneria Aerospaziale Internal Report, Rome, Italy, June 2005.

[15] Giulietti, D., and Lucchesi, M., "Emissivity and Absorptivity Measurements on Some High-Purity Metals at Low Temperature," *Journal of Physics D: Applied Physics*, Vol. 14, No. 5, 1981, pp. 877–881.

[16] Rowe, W. M., Luedke, E. E., and Edwards, D. K., "Thermal Radiative Properties of Solar Sail Film Materials,"*AIAA and ASME Thermophysics and Heat Transfer Conference, 2nd*, AIAA Paper 78-852, Palo Alto, CA, 24–26 May 1978.

[17] Stimpson, L. D., Greenfield, M. L., Jaworski, W., and Wolf, F., "Thermal Control of a Solar Sail," *American Institute of Aeronautics and Astronautics and American Society of Mechanical Engineers, Thermophysics and Heat Transfer Conference, 2nd*, AIAA Paper 78-885, Palo Alto, CA, 24–26 May 1978.

[18] Dachwald, B., and Wie, B., "Solar Sail Trajectory Optimization for Intercepting, Impacting, and Deflecting Near-Earth Asteroids," *AIAA Guidance, Navigation, and Control Conference and Exhibit*, AIAA Paper 2005-6176, San Francisco, 15–18 Aug. 2005.

[19] Wood, L. J., Bauer, T. P., and Zondervan, K. P., "Comment on 'Time-Optimal Orbit Transfer Trajectory for Solar Sail Spacecraft'," *Journal of Guidance, Control, and Dynamics*, Vol. 5, No. 2, March–April 1982, pp. 221–224.

[20] Lawden, D. F., *Optimal Trajectories for Space Navigation*, Butterworths, London, 1963, pp. 54–68.

[21] Sauer, C. G., Jr., "Optimum Solar-Sail Interplanetary Trajectories," *AIAA/AAS Astrodynamics Conference*, AIAA Paper 76-0792, San Diego, CA, 18–20 Aug. 1976.

[22] Dachwald, B., "Minimum Transfer Times for Nonperfectly Reflecting Solar Sailcraft," *Journal of Spacecraft and Rockets*, Vol. 41, No. 4, July–Aug. 2004, pp. 693–695.